Hindawi
Advances in Civil Engineering
Volume 2022, Article ID 1315213, 16 pages
https://doi.org/10.1155/2022/1315213

Research Article

Vibration Reduction Performance of Structures with Viscous Dampers under Near-Field Earthquakes

Jianguang Lin

Fujian Provincial Institute of Architectural Design and Research Co., Ltd, Fuzhou 350001, China

Correspondence should be addressed to Jianguang Lin; 2150392433@qq.com

Received 10 June 2022; Accepted 22 August 2022; Published 30 September 2022

Academic Editor: Wen-Shao Chang

Copyright © 2022 Jianguang Lin. This is an open access article distributed under the Creative Commons Attribution License, which permits unrestricted use, distribution, and reproduction in any medium, provided the original work is properly cited.

Near-field pulse-type ground motions (NPGMs) are characterized by a high-energy pulse with large peak ground velocities and accelerations and need further studies to confirm whether structures with viscous dampers (VDs) are still applicable and effective for this type of ground motions. In this article, the vibration reduction performance of structures with VDs under near-field earthquakes is investigated systematically. Displacement and acceleration spectra are developed for a single-degree-of-freedom (SDOF) structure with and without VDs, while these influence factors, such as the nonlinear characteristic of structure, damper supports' flexibility, and damper parameters, are considered. Additionally, the frequency domain characteristics of NPGM and the energy distribution of a multidegree-of-freedom (MDOF) structure with VDs are discussed to further reveal the action mechanism of NPGM on the structure. It is shown that the structure with VDs shows remarkable seismic reduction effect under the action of near-fault pulse-type earthquake, and the maximum interstorey drift decreased from 0.086 to 0.037 when the structure is equipped with VDs. However, the structure may still be difficult to completely dissipate the high-energy generated by the earthquake pulse with a high pulse period in a short time, which can cause the structure to be damaged or even collapsed in a moment.

1. Introduction

In recent years, considerable passive energy dissipation devices, such as viscoelastic dampers, metallic yield dampers, friction dampers, and fluid viscous dampers [1], have been widely applied in structures to enhance their energy dissipation capability, which can reduce the seismic response of the structure under ordinary ground motions obviously [2, 3]. Among these devices, fluid viscous dampers are more prevalent due to its wide frequency band of vibration attenuation [4], low cost, and easy maintenance. However, in recent major earthquakes (Northridge 1994, Chi-Chi 1999) [5–7], a type of near-field pulse-type ground motion (NPGM) has been found. It is characterized by a high-energy pulse with large peak ground velocities and accelerations, which can cause more serious damage to structures than ordinary ground motions, and many research literature studies [8–12] have confirmed this adverse effect. Therefore, whether structures with viscous dampers (VDs) are still applicable and effective for this special type of ground motions needs further study.

It has to be recognized that, for strong earthquakes, most structures employing VDs will experience some level of inelastic response [13], which may cause significant increases in the base shear; therefore, the nonlinear influence of structures on the seismic responses should be considered. Kumar [14] investigated the seismic performance of multistorey structures strengthened with nonlinear viscous dampers. Güler and Alhan [15] compared the seismic performance of the base-isolated liquid storage tanks with/without supplemental damping. Yaghmaei-Sabegh et al. [16] proposed a modified direct method to estimate the seismic response of structures equipped VDs under near-field pulse-like ground motions. Xu et al. [17] investigated the performance of an SDOF structure with VDs when it is subjected to NPGM, and the conclusion indicated that the structural displacement can be reduced significantly when the ratio of structure to excitation periods is in a certain range. Yi et al. [18] proposed to use a negative stiffness device combined with FVD for the bridge and investigated the seismic response of the bridge under near-fault earthquakes.

The results indicated that the acceleration and the deck displacement of the bridge can be reduced.

This article extends Ref. [17], which focuses on the vibration reduction performance of structures with VDs under near-field earthquakes, and these influence factors such as the nonlinear characteristic of structure, damper supports' flexibility, and damper parameters are considered. The state-space representation is used to describe structures with VDs, and the seismic response of the structure under four groups of NPGM with different pulse periods is calculated and compared. Furthermore, the dissipated energy distribution of the structure and the frequency domain characteristics of NPGM are employed to further reveal the action mechanism of NPGM on the structure.

2. Modelling of Structures with VDs in State-Space Representation

2.1. SDOF. An SDOF structure with VDs is presented in Figure 1(a), where the supplementary VD is connected to the structure through a linear elastic supporting brace, and the Maxwell model is used to describe its mechanical behaviour. It is comprised of a purely viscous damper with damping coefficient c_d and a purely elastic spring with stiffness k_b. Figures 1(b) and 1(c) show the prototype of viscous damper.

The dynamic equation of an SDOF structure with VDs subjected to ground motion $\ddot{x}_\mathrm{g}$ can be described by means of the following equation:

$$m\ddot{x} + c\dot{x} + kx + k_b\left(x - x_d\right) = -m\ddot{x}_\mathrm{g}, \tag{1}$$

where m, c, and k are the structural mass, inherent damping coefficient, and lateral stiffness, respectively; and x, $\dot{x}$, and $\ddot{x}$ represent the responses of displacement, velocity, and acceleration, respectively. Note that x consists of two parts: the displacement x_d of VD and the elastic deformation of the supporting brace. In the following, the exponent α_0 of VD controls the damper nonlinearity and its typical values is in the range of 0.2–1 [3, 19–21] for seismic applications:

$$c_d\left|\dot{x}_d\right|^{\alpha_0}\mathrm{sgn}\left(\dot{x}_d\right) = k_b\left(x - x_d\right). \tag{2}$$

In this article, the influence of α_0 in the range of 0.3–1 on the vibration reduction performance of the structure has been discussed.

Assuming that the brace stiffness k_b is proportional to the lateral stiffness k of the structure, and the damper coefficient c_d is proportional to the damping c of the structure [22], two dimensionless parameters can be respectively defined as

$$\alpha = \frac{k_b}{k}, \beta = \frac{c_d}{c}. \tag{3}$$

Hence, k_b and c_d can be replaced by the above equation [23], and the resulting equation is divided by m to obtain the following:

$$\ddot{x} + 2\omega\xi\dot{x} + \omega^2 x + \alpha\omega^2\left(x - x_d\right) = -\ddot{x}_g \tag{4}$$

$$\frac{k_b}{c_\mathrm{d}\omega} = \frac{\alpha}{2\beta\xi}, \tag{5}$$

where $\omega = \sqrt{k/m}$ and $\xi = c/2m\omega$ are the circular frequency and the damping ratio of the structure, respectively. For the convenience of calculating the seismic response of the structure, the state-space representation has been used to transform second-order differential equations (4) and (5) into first-order differential equations and the structural displacement; velocity and the VD's displacement are selected as state variables, which is shown in the following equation:

$$\dot{y} + A_0 y + B_0\ddot{x}_g + C_0 = 0, \tag{6}$$

where y is a column vector of the equations; A_0, B_0, and C_0 are the supplementary matrix with constant elements, respectively, which can be written as

$$y = \begin{bmatrix} x \\ \dot{x} \\ x_\mathrm{d} \end{bmatrix},$$

$$\dot{y} = \begin{bmatrix} \dot{x} \\ \ddot{x} \\ \dot{x}_\mathrm{d} \end{bmatrix},$$

$$A_0 = \begin{bmatrix} 0 & -1 & 0 \\ (1+\alpha)\omega^2 & 2\omega^2\xi & -\alpha\omega^2 \\ 0 & 0 & 0 \end{bmatrix}, \tag{7}$$

$$B_0 = \begin{bmatrix} 0 \\ 1 \\ 0 \end{bmatrix},$$

$$C_0 = -\begin{bmatrix} 0 \\ 0 \\ 1 \end{bmatrix}\mathrm{sgn}\left(x - x_\mathrm{d}\right)\left|\frac{\alpha\omega}{2\beta\xi}\left(x - x_\mathrm{d}\right)\right|^{1/\alpha_0}.$$

Note that all the variables change with $\ddot{x}_\mathrm{g}$, which vary with time at a high rate, and equation (5) contains a series of stiff equations; therefore, Gear's backward numerical differential algorithm is chosen to solve the equations.

However, when the structure enters into an elastoplastic state under strong earthquake, the influence of stiffness degradation on the seismic response of the structure should be considered, and therefore, the frequently used bilinear elastoplastic model (Figure 2) has been employed to describe

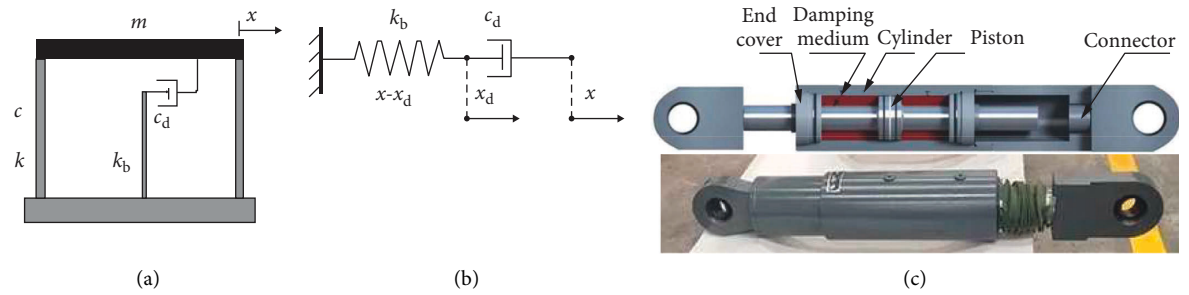

Figure 1: (a) Model for the SDOF system with VDs; (b) Maxwell model; (c) prototype of viscous damper.

the nonlinear characteristic of the structure. Now equation (1) of an SDOF structure with VDs can be rewritten as

$$m\ddot{x} + c\dot{x} + f(x) + k_b(x - x_d) = -m\ddot{x}_g \tag{8}$$

At the same time, the strength reduction factor R and ductility factor μ are defined as

$$R = \frac{f_e}{f_y} = \frac{mS_a}{f_y}, u = \frac{x}{x_y}\left(x_y \le x\right), \tag{9}$$

where R is the ratio of the maximum elastic force mS_a to the yield force f_y of the structure, S_a is the structural maximum elastic acceleration, and the yield force f_y can be expressed as $f_y = k_e x_y$; u is the ratio of the maximum inelastic displacement x to the yield displacement x_y of the structure, and $f(x)$ is the elastoplastic restoring force. In order to obtain the inelastic seismic response of the structure under the condition of equal strength or equal ductility, the x in equation (8) can be replaced by equation (9); thus, a new equation is defined as

$$\ddot{u} + 2\xi\omega\dot{u} + \omega^2\frac{f(x)}{f_y} + \alpha\omega^2\left(u - \frac{\omega^2 R x_d}{S_a}\right) = -\frac{\omega^2 R}{S_a}\ddot{x}_g \tag{10}$$

Based on equations (10) and (2), the inelastic seismic response of the structure can be obtained with the state-space method when R is determined.

2.2. MDOF. For a n-storey structure equipped with VDs at each storey, the bilinear elastoplastic model has been used to describe the characteristic of cyclic behaviour of the structure in each storey at the same time, and its dynamic equation can be expressed as

$$M\ddot{X} + C\dot{X} + F(X) + F_D(X) = -MI\ddot{x}_g \tag{11}$$

where M and C are the $n \times n$ structural mass and damping matrices; X is the $n \times 1$ vector of structural displacements; $F(X)$ is the $n \times 1$ vector of the elastoplastic restoring forces; and I is a $n \times 1$ unity vector; $F_D(X)$ is the $n \times 1$ vector of damper forces. Now the state-space representation has been employed to convert equation (11) into an array of first-order ordinary differential equations, which is shown as

$$\dot{Z} + \mathbf{A}_1 Z + \mathbf{B}_1\ddot{x}_g + \mathbf{C}_1 = \mathbf{0}, \tag{12}$$

where the state variable Z is a $3n \times 1$ vector that contains the structural displacements X, velocities $\dot{X}$, and plastic displacement components U; the matrices $\mathbf{A}_1, \mathbf{B}_1$, and C_1 are auxiliary conversion matrices, which can be determined as follows:

$$Z = \begin{bmatrix} X \\ \dot{X} \\ U \end{bmatrix}$$

$$\dot{Z} = \begin{bmatrix} \dot{X} \\ \ddot{X} \\ \dot{U} \end{bmatrix},$$

$$\mathbf{A}_1 = \begin{bmatrix} \mathbf{0} & \mathbf{E} & \mathbf{0} \\ \dfrac{K_e}{M} & \dfrac{C}{M} & \dfrac{K_p}{M} \\ \mathbf{0} & \mathbf{0} & \mathbf{0} \end{bmatrix},$$

$$\mathbf{B}_1 = \begin{bmatrix} \mathbf{0} \\ I \\ \mathbf{0} \end{bmatrix}, \tag{13}$$

$$\mathbf{C}_1 = \begin{bmatrix} \mathbf{0} \\ \dfrac{F_D}{M} \\ p \end{bmatrix},$$

$$F_D = \begin{bmatrix} f_1 - f_2 \\ \vdots \\ f_n \end{bmatrix},$$

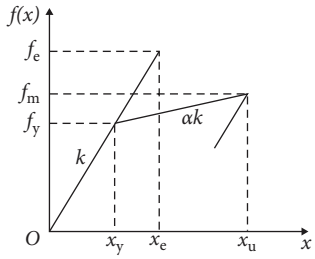

Figure 2: Bilinear elastoplastic model.

where K_e and K_p are the $n \times n$ structural elastic stiffness and plastic stiffness matrices, respectively; **0** and **E** are the $n \times n$ zero matrices and unity matrices, respectively; p is a $n \times 1$ vector, which represents the plastic hysteretic characteristics of the structure; f_i is the damper force for the i-th storey, and it can be written as

$$f_i = c_{di}\left|x_i - x_{i-1}\right|^{\alpha_0} \operatorname{sgn}\left(x_i - x_{i-1}\right) (i = 2, 3, \cdots n). \tag{14}$$

Combining equations (12) and (14) and using Gear's backward numerical differential algorithm to solve the equations, the inelastic seismic response of the MDOF structure with VDs under strong earthquakes can be obtained.

3. Selection of NPGM

Based on the method of regionalization of near-field seismic region proposed by Ming [24], a number of near-field ground motions of strike-slip faults mechanism with moment magnitude M_w greater than 5.5 were selected from the Pacific Earthquake Engineering Research (PEER) Center. Then, a pulse indicator PI was proposed by Baker [25], which has been employed to identify whether a given record is pulse-like. PI shown in equation (15) takes values between 0 and 1, with a higher value indicating that the record is pulse-like, and the record can be classified as pulse when PI is greater than 0.85. The PGV ratio is the value of the peak ground velocity (PGV) of the residual record divided by the original record's PGV, and the energy ratio is the value of the energy of the residual record divided by the original record's energy [25]:

$$PI = \frac{1}{1 + e^{-23.3+14.6\,(\text{PGVratio})+20.5\,(\text{energyratio})}}. \tag{15}$$

Finally, 24 pulse-type ground motions have been picked out based on the above method and divided into four groups (G1~G4) in accordance with its pulse period PI. The four groups can be defined as follows: when $0.5\text{s} \le PI \le 1.1\text{s}$, the ground motions are classified as the G1 group; when $2.0\text{s} \le PI \le 2.9\text{s}$, the ground motions are classified as the G2 group; when $4.0\text{s} \le PI \le 4.6\text{s}$, the ground motions are classified as the G3 group; when $5.1\text{s} \le PI \le 6.0\text{s}$, the ground motions are classified as the G4 group, which are shown in Table 1.

4. Analysis of the Influence Factors and Vibration Reduction Performance

4.1. Analysis of Influence Factors

4.1.1. Influence of the Parameters of VD. It is clear to see that the seismic response of the structure varies directly with the values of k_b, α, β, α_0, and α_1 on the basis of equations (4), (5), and (8). Thus, before further studying on the vibration reduction performance of the whole structure, we should understand the influence of these parameters on the seismic response of the structure in detail. In order to clarify the characteristics of its influence, now record no. n1114 obtained from the 1995 Kobe Japan earthquake is selected as excitation, and the seismic response of an elastic SDOF structure with VDs (ETD) and its corresponding uncontrolled structure (UST) are calculated.

Figures 3(a) and 3(b) show the curves of the displacement ratios of ETD to UST varying with the parameters $k_b/(c_d\omega)$ and α_0 for different structural periods (T = 0.6s and 2.0s, which represent the short period structure and the long period structure, respectively), and Figures 3(c) and 3(d) show the varied curves of the acceleration ratios of the corresponding structures mentioned above. Here, x_m and x_0 are the maximum elastic displacement responses of ETD and UST, respectively. $\ddot{x}_m$ and $\ddot{x}_0$ are the maximum elastic acceleration responses of ETD and UST, respectively. It is observed from Figures 3(a) and 3(b) that x_m/x_0 decreases with an increase in $k_b/(c_d\omega)$ when β equals 2, which indicates that the vibration reduction effect of ETD can be improved by increasing the value of $k_b/(c_d\omega)$ within a certain range and the effect can remain stable when $k_b/(c_d\omega)$ exceeds the range. Furthermore, it can be found that the vibration reduction effect will be more significant when the exponent α_0 of the VD is smaller and the structural period T is shorter. However, with the period T increasing from 0.6 s to 2.0 s (the corresponding circular frequency ω decreasing from 10.47 to 3.14), the difference of influence of α_0 with different values on the vibration reduction effect of ETD gradually decreased. When T equals 2.0 s, the effect is basically the same no matter what value α_0 takes in the range of 0.3–1.0. It can be clearly found that the acceleration response of the structure has also the similar change rule, as shown in Figures 3(c) and 3(d).

Moreover, Figures 3(e) and 3(f) show the corresponding displacement ratios of VD to ETD. It can also be observed that the ratio of x_d/x_m varies with the change of $k_b/(c_d\omega)$ and α_0. For a damper with a smaller exponent α_0, a larger value of $k_b/(c_d\omega)$ is needed when the displacement x_d of the damper becomes closer to the displacement of the structure, namely, $x_d/x_m \approx 1.0$. But with the increase in the period T, the influence of α_0 on the minimum value of $k_b/(c_d\omega)$, which keeps the ratio of x_d/x_m constant, is gradually weakened.

Based on the above analysis, it is recommended that the minimum range of $k_b/(c_d\omega)$, which can help to take full use of the energy dissipation capacity of the damper, is between 3 and 6 for the different values of α_0 and periods T of the

Table 1: Near-field pulse-type ground motions.

Group	No.	Ground motion	Component	Pulse period PI	Group	No.	Ground motion	Component	Pulse period PI
G1	n569	San Salvador	NGI270	1.02	G2	n20	Northern Calif-03	FRN044	2.05
	n1602	Duzce Turkey	BOL090	0.88		n158	Imperial Valley-06	AEP045	2.44
	n4102	Parkfield-02 CA	C03360	1.02		n159	Imperial Valley-06	AGR003	2.45
	n4103	Parkfield-02 CA	C04090	0.62		n173	Imperial Valley-06	E10320	2.06
	n4126	Parkfield-02 CA	SC1090	0.64		n569-1	San Salvador	NGI180	2.33
	n4126	Parkfield-02 CA	SC1360	0.57		n1114	Kobe Japan	PRI000	2.83
G3	n161	Imperial Valley-06	BRA225	4.24	G4	n6906	Darfield New Zealand	GDLCS35 W	2.24
	n170	Imperial Valley-06	ECC092	4.31		n183	Imperial Valley-06	E08230	5.39
	n180	Imperial Valley-06	E05230	4.13		n184	Imperial Valley-06	EDA270	5.97
	n182	Imperial Valley-06	E07230	4.28		n185	Imperial Valley-06	HVP225	5.15
	n1176	Kocaeli Turkey	YPT150	4.54		n316	Westmorland	PTS225	5.36
	n6911	Darfield New Zealand	HORCS72 E	4.02		n1176-1	Kocaeli Turkey	YPT060	5.12

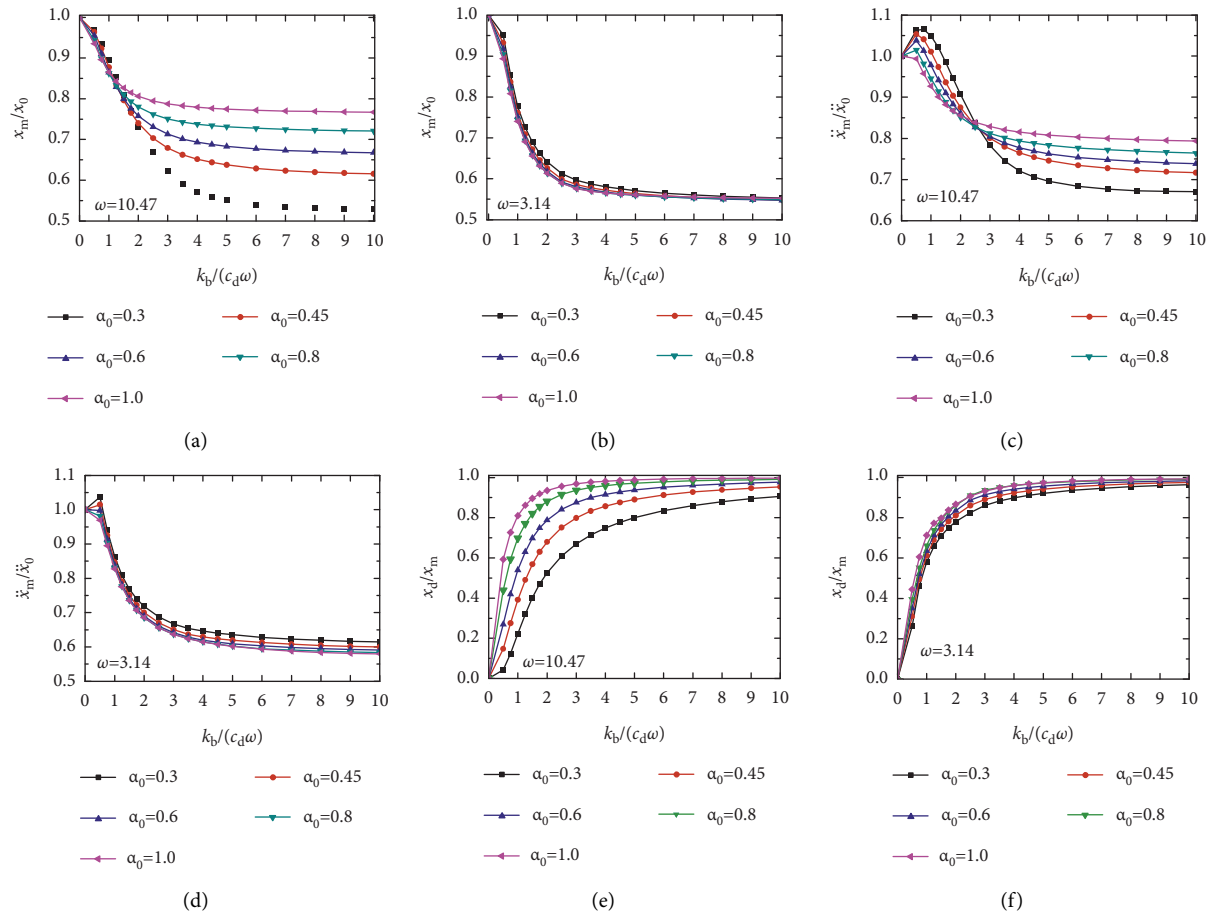

Figure 3: Influence of the parameters $k_b/(c_d\omega)$ and α_0 on the seismic response of the SDOF structure ($\beta = 2$) with periods T equals 0.6 s and 2.0 s, respectively: (a)-(b) the displacement ratios of ETD to UST; (c)-(d) the acceleration ratios of ETD to UST; (e)-(f) the displacement ratios of VD to ETD.

structure. Namely, the minimum value of $k_b/(c_d\omega)$ should not be less than 6 when α_0 equals 0.3, and $k_b/(c_d\omega)$ should not be less than 3 when α_0 equals 1.0, which can help to make full use of the energy dissipation capacity of dampers. When α_0 is between 0.3 and 1.0, $k_b/(c_d\omega)$ can be determined by linear interpolation. Once the value of $k_b/(c_d\omega)$ is

determined, the minimum value of k_b can also be determined according to the structural period T and the coefficient c_d of VD.

In addition, in order to further illustrate the influence of β on the vibration reduction effect of ETD, Figures 4(a) and 4(b) show the curves of the displacement ratios of ETD to UST varying with the parameters $k_b/(c_d\omega)$ and β when the natural vibration period T of the structure equals 2.0 s. Figures 4(c) and 4(d) show the curves of the acceleration ratios of the corresponding structures mentioned above. Figures 4(e) and 4(f) show the curves that the corresponding displacement ratios of VD to ETD. It can be observed from Figures 4(a)–4(d) that x_m/x_0 and $\ddot{x}_m/\ddot{x}_0$ decrease significantly with the increase of β, which indicates that the vibration reduction effect of the structural displacement and acceleration is remarkable, and the ratios of x_d/x_m have the similar changing trends and less affected by the different values of β and α_0, as shown in Figures 4(e) and 4(f). Besides, it has to be noted that whether the energy dissipation capacity of the damper can be sufficiently utilized mainly depends on the parameter $k_b/(c_d\omega)$, which is relative stable and dimensionless. It is observed that the linear VD ($\alpha_0 = 1.0$) can be sufficiently utilized and is almost not affected by the damper coefficient c_d and other influence factors when $k_b/(c_d\omega)$ equals 3; while for the nonlinear VD ($0.3 \le \alpha_0 < 1.0$), the minimum value of $k_b/(c_d\omega)$ is affected by the parameters α_0 and β. Namely, a smaller exponent α_0 and a higher coefficient β usually require a larger value of $k_b/(c_d\omega)$, which can contribute to making full use of the energy dissipation capacity of the damper. Nevertheless, when $k_b/(c_d\omega)$ equals 6, the nonlinear VD ($\alpha_0 = 0.3$) can basically be fully utilized, which indicate that the range of $k_b/(c_d\omega)$ between 3 and 6 is suitable for the change of exponent α_0 in the range of 0.3–1.0.

4.1.2. Influence of Other Factors. Additionally, it is well known that the ground motions are characterized by great uncertainty; therefore, different ground motions have been selected as excitations and the seismic responses of the structure with VDs are calculated and compared according to the above methods. It can be found that the influence of these parameters on the structure under different ground motions is similar to the above analyzed conclusions, which can be used to demonstrate that the influence rules mentioned above are general. However, it should be realized that the demands for dampers of the structure under different ground motions are different, and sometimes, the amount of the dampers are excessive when the structure is subjected to some near-fault ground motions, which may lead to amplify the acceleration response of the structure although the displacement response of the structure can be reduced, as shown in Figures 5(a) and 5(b). The results confirm that an optional damping is needed to balance the reduction of structural displacement and the increase of the total acceleration [14].

At the same time, the influence of stiffness degradation on the seismic response of the structure is considered, and the displacement response spectra SD of an SDOF structure with and without VDs are compared, as shown in Figure 5(c). It can be observed that the inelastic displacement of the uncontrolled structure shows a certain degree of discreteness relative to the elastic displacement when the structure enters into an elastoplastic state; however, when it is equipped with VDs, the displacement of the structure shows no obvious change in the elastic state and the elastoplastic state. The result indicates that the damper can effectively restrain the adverse effects of discrete deformation caused by stiffness degradation when the structure enters into an elastoplastic state.

4.2. Analysis of Pulse-Type Spectra. Now these parameters of $k_b/(c_d\omega) = 6$, $\beta = 4$, and $\alpha_0 = 0.3$ are determined on the basis of the above conclusions, which have been used to calculate spectra for an elastic SDOF structure with VDs (ETD) and an elastoplastic SDOF structure ($R = 4$) with VDs (PTD) when the structure is subjected to NGPM, which is shown in Table 1; at the same time, the spectra for an uncontrolled SDOF structure (UST) are also given as a contrast, and the spectra in the range of 0.1–10 s are shown in Figure 6. Additionally, two dimensionless displacement coefficients (β_{sd1} and β_{sd2}) and two dimensionless acceleration coefficients (β_{sa1} and β_{sa2}) are defined as

$$\begin{aligned}
\beta_{sd1} &= \frac{\mathrm{SD(ETD)}}{\mathrm{SD(UST)}},\\
\beta_{sd2} &= \frac{\mathrm{SD(PTD)}}{\mathrm{SD(UST)}},\\
\beta_{sa1} &= \frac{\mathrm{SA(ETD)}}{\mathrm{SA(UST)}},\\
\beta_{sa2} &= \frac{\mathrm{SA(PTD)}}{\mathrm{SA(UST)}},
\end{aligned} \tag{16}$$

where SD(UST), SD(ETD), and SD(PTD) are the spectral displacement of UST, ETD, and PTD, respectively; SA(UST), SA(ETD), and SA(PTD) are the corresponding spectral acceleration.

It is observed from Figures 6(a) and 6(d) that SD increases with an increase in T_p, and the peak displacement response occurs when $T \approx T_p$. Meanwhile, the attenuation rate of SA slows down with an increase in T_p. However, when the structure is equipped with VDs, a quite different vibration reduction effect of ETD is presented in different period ranges, as shown in Figures 6(b) and 6(e). For the ground motions of the G1 group, the vibration reduction effect of SD is remarkable when T is between 0.1 s and 2.0 s, but once it goes out of this range, the displacement of ETD will not be significantly reduced or even amplified. Moreover, the acceleration response of ETD is also amplified when T is more than 1.0 s, which indicates that only in a certain range of period can the energy dissipation capacity of the damper be utilized efficiently when the structure is subjected to NPGM with pulse periods less than

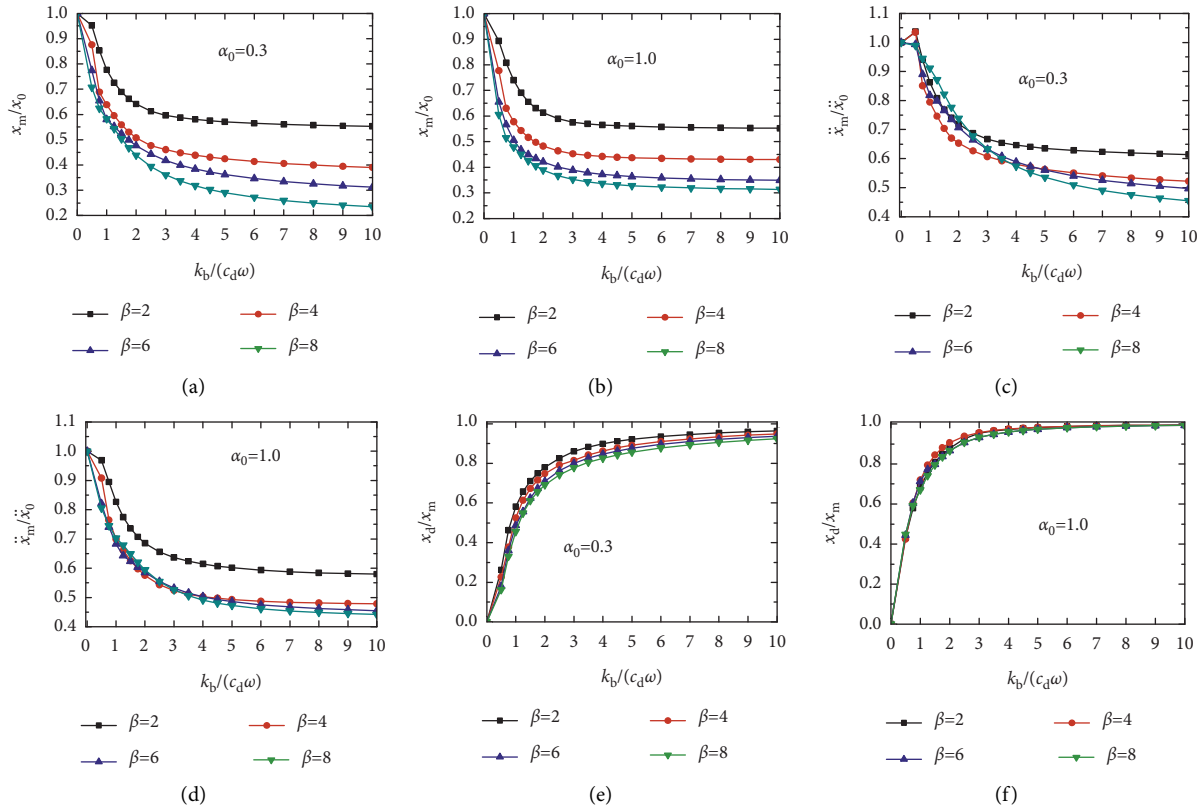

FIGURE 4: Influence of the parameter β on the seismic response of the SDOF structure (T = 2.0s) with the exponent α_0 equal to 0.3 and 1.0: (a)-(b) the displacement ratio of ETD to UST; (c)-(d) the acceleration ratio of ETD to UST; (e)-(f) the displacement ratio of VD to ETD.

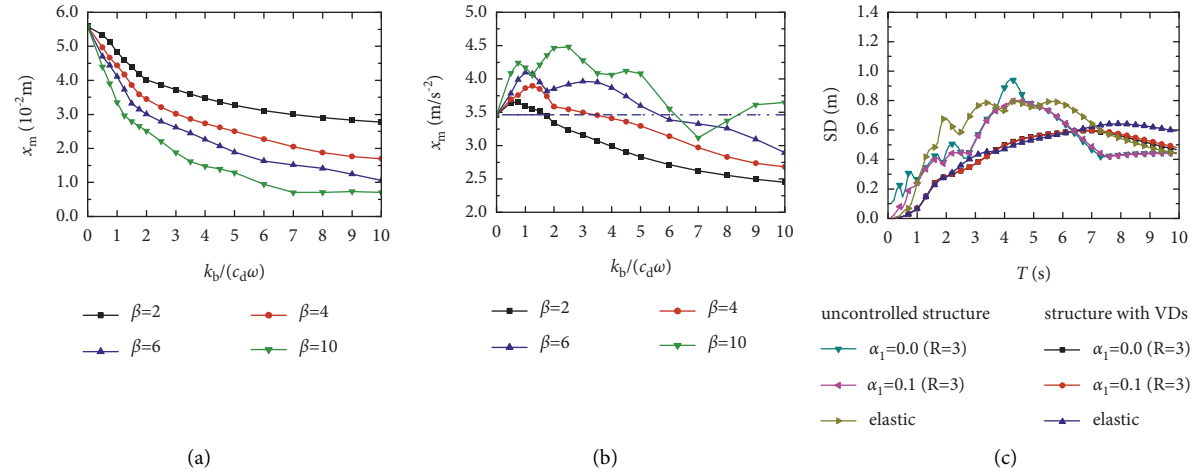

FIGURE 5: The seismic response of the SDOF structure with the different values of β: (a) the displacement of ETD; (b) the acceleration ratios of ETD; (c) the displacement response spectra of the uncontrolled structure and the structure with VDs.

1.0 s. For the ground motions of G2~G4 groups, SD and SA increase with an increase in T_p, which can lead to an increase in demands for dampers at the same time and that enables the damper to be utilized efficiently in a wider range of period. The displacement response of PTD shows no apparent change relative to that of ETD when the structure enters into an elastoplastic state, but its corresponding structural acceleration response is slightly reduced, as shown in Figures 6(c) and 6(f), which indicates that the adverse effect of stiffness degradation on the seismic response of PTD can be significantly reduced when the structure is equipped with VDs. Moreover, the similar results can also be obtained with different β and α_0 values, and R changes in the range of 2–8.

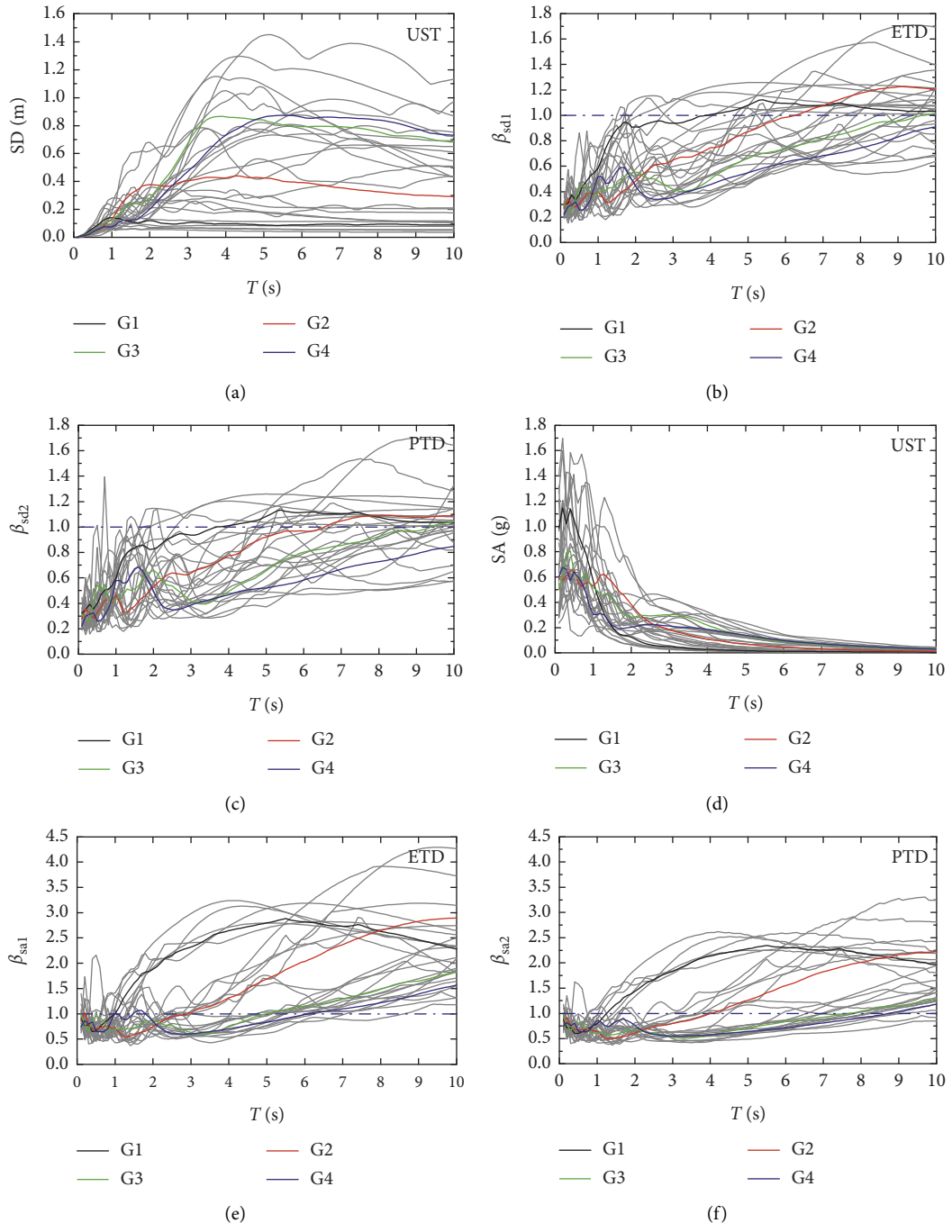

Figure 6: Displacement and acceleration spectra for different SDOF structures: (a)-(c) displacement spectra for UST, ETD, and PTD ($R = 4$), respectively; (d)-(f) acceleration spectra for UST, ETD, and PTD ($R = 4$), respectively.

Figure 7 shows the plots of the normalized spectra of SD and SA as the function of period ratio T/T_p for ETD and PTD ($R = 4$) subjected to NPGM. Figures 7(a) and 7(b) show β_{sd1} and β_{sd2} normalized displacement spectra for ETD and PTD, respectively. It is observed from Figures 7(a) and 7(b) that the reduction in displacement is not obvious when $T/T_p < 0.5$, even amplified for PTD, and relative higher reduction can be obtained for $0.5 < T/T_p < 1.5$. However, the displacement response of ETD and PTD shows great discreteness when $T/T_p > 1.5$.

Figures 7(c) and 7(d) show β_{sa1} and β_{sa1} normalized acceleration spectra for ETD and PTD ($R = 4$), respectively. It is observed from Figures 7(c) and 7(d) that the characteristic of reduction in acceleration is similar; that is, reduction in acceleration is not obvious when $T/T_p < 0.5$, and most of acceleration responses are amplified. However, larger reduction can be obtained for $0.5 < T/T_p < 1.5$, and it is amplified for both elastic and elastoplastic structures when $T/T_p > 1.5$.

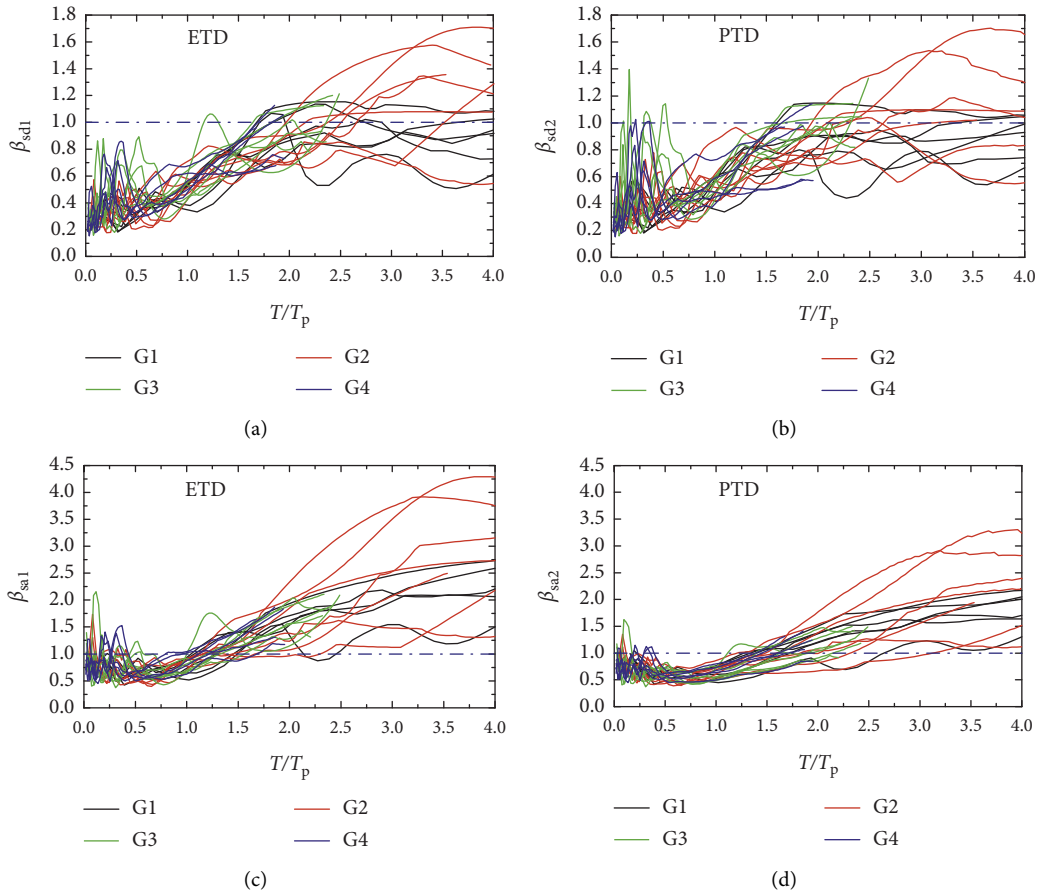

FIGURE 7: Normalized displacement and acceleration spectra for ETD and PTD ($R = 4$): (a)-(b) normalized displacement spectra for ETD and PTD, respectively; (c)-(d) normalized acceleration spectra for ETD and PTD, respectively.

4.3. Energy Response of Pulse-Type Excitation. To investigate the energy distribution characteristic of structure with VDs when it subjected to NPGM, the energy balance approach has been employed to analyze the cumulative energy response for the structure. The cumulative energy response for the structure in equation (8) can be obtained by integrating (8) with a displacement increment dx as

$$\int_0^t m\ddot{x}\mathrm{d}x + \int_0^t c\dot{x}\mathrm{d}x + \int_0^t f(x)\mathrm{d}x + \int_0^t k_b(x - x_d)\mathrm{d}x = -\int_0^t m\ddot{x}_g\mathrm{d}x, \tag{17}$$

$$E_K = \int_0^t m\ddot{x}\mathrm{d}x,$$
$$E_D = \int_0^t c\dot{x}\mathrm{d}x, \tag{18}$$
$$E_S + E_H = \int_0^t f(x)\mathrm{d}x,$$

where each integral expression represents the cumulative energy from 0 to t time. The first and second terms on the left side of equation (17) represent kinetic energy $E_K$and inherent damping energy E_D, respectively, and the third term is the strain energy, which includes elastic strain energy E_S and plastic strain energy E_H. The fourth term on the left side of equation (17) is the energy dissipated by VD, and it can be calculated as

$$E_V = \int_0^t k_b(x - x_d)\mathrm{d}x = \int_0^t c_d|\dot{x}_d|^{\alpha_0}\mathrm{sgn}(\dot{x}_d)\mathrm{d}x. \tag{19}$$

The total seismic input energy E_{inp} on the right side of equation (17) can be written as

$$E_{inp} = -\int_0^t m\ddot{x}_g\mathrm{d}x. \tag{20}$$

Figure 8 shows time-history plots of the accumulative energy response that include seismic input, kinetic, inherent damping, strain, and dissipated energies for an uncontrolled SDOF structure and the structure with VDs subjected to pulse excitation. It is observed from Figure 8(a) that, for the uncontrolled structure, the seismic input energy of ground motions is dissipated mainly by plastic strain energy and inherent damping energy once the structure enters into an elastoplastic state, which indicates that it may suffer severe damage. While for the structure with VDs, the total input energy is dissipated mainly by the hysteresis energy of VD as shown in Figure 8(b), and the proportion of plastic strain energy to total input energy is significantly reduced.

Figure 9 shows the plots of the max seismic input energy E_{inp} as a function of T/T_p for structures subjected to some pulse excitations. In Figure 9, β_E represents the ratio of the max seismic input energy E_{inp} of structure with VDs to the uncontrolled structure. It is observed from Figure 9(a) that peak input energy E_{inp} of the uncontrolled structure occurs when $0.5 < T/T_p < 1.0$.

When structure is equipped with VDs, a smaller value of β_E in the range of $0.5 < T/T_p < 1.0$ can be found, which implies that the most significant reduction in seismic input energy occurs when$0.5 < T/T_p < 1.0$, while the input energy of structure with VD is amplified when $T/T_p < 0.5$, which is shown in Figure 9(b). This can be used to explain why the seismic response of the structure with VDs in Figures 7(b) and 7(d) is not reduced or even amplified when $T/T_p < 0.5$.

5. Numerical Example

In order to further reveal the action mechanism of near-fault ground motions on structure with VDs, a characteristic twelve-storey steel frame is presented, as shown in Figure 10, whose seismic performance has met the requirement of the Chinese design code (GB50011). The bottom storey height is equal to 4.0 m and the others are 3.6 m, and all the materials are standard steel grade Q355. Columns consist of standard BOX sections, beams consist of standard middle flange H-type sections (HM) and narrow flange H-type sections (HN), and the more detailed information is presented in Table 2. The frame is subjected to a uniform floor dead load 4.7 kN/m^2 on each storey. The floor live load is 4.0 kN/m^2 for the first to sixth storeys and 2.0 kN/m^2 for the seventh to twelfth storeys. Furthermore, the bilinear elastoplastic model has been used to describe the characteristic of nonlinear behaviour of the structure, and the ratio of postyielding stiffness to elastic stiffness of the structure is 0.02.

The condensed elastic stiffness matrix K_e and plastic stiffness matrix K_p of the structure can be expressed as

$$K_e = \begin{bmatrix} 9.90 & -3.54 & 0 & 0 & 0 & 0 & 0 & 0 & 0 & 0 & 0 & 0 \\ -3.54 & 6.50 & -2.96 & 0 & 0 & 0 & 0 & 0 & 0 & 0 & 0 & 0 \\ 0 & -2.96 & 5.65 & -2.69 & 0 & 0 & 0 & 0 & 0 & 0 & 0 & 0 \\ 0 & 0 & -2.69 & 5.18 & -2.49 & 0 & 0 & 0 & 0 & 0 & 0 & 0 \\ 0 & 0 & 0 & -2.49 & 4.91 & -2.42 & 0 & 0 & 0 & 0 & 0 & 0 \\ 0 & 0 & 0 & 0 & -2.42 & 4.79 & -2.37 & 0 & 0 & 0 & 0 & 0 \\ 0 & 0 & 0 & 0 & 0 & -2.37 & 4.70 & -2.33 & 0 & 0 & 0 & 0 \\ 0 & 0 & 0 & 0 & 0 & 0 & -2.33 & 4.35 & -2.02 & 0 & 0 & 0 \\ 0 & 0 & 0 & 0 & 0 & 0 & 0 & -2.02 & 4.07 & -2.04 & 0 & 0 \\ 0 & 0 & 0 & 0 & 0 & 0 & 0 & 0 & -2.04 & 4.04 & -2.00 & 0 \\ 0 & 0 & 0 & 0 & 0 & 0 & 0 & 0 & 0 & -2.00 & 3.75 & -1.74 \\ 0 & 0 & 0 & 0 & 0 & 0 & 0 & 0 & 0 & 0 & -1.74 & 1.74 \end{bmatrix} \times 10^5 \text{kN/m},$$

$$K_p = \begin{bmatrix} 9.97 & -5.00 & 0 & 0 & 0 & 0 & 0 & 0 & 0 & 0 & 0 & 0 \\ 0 & 5.00 & -4.17 & 0 & 0 & 0 & 0 & 0 & 0 & 0 & 0 & 0 \\ 0 & 0 & 4.17 & -3.80 & 0 & 0 & 0 & 0 & 0 & 0 & 0 & 0 \\ 0 & 0 & 0 & 3.80 & -3.51 & 0 & 0 & 0 & 0 & 0 & 0 & 0 \\ 0 & 0 & 0 & 0 & 3.51 & -3.42 & 0 & 0 & 0 & 0 & 0 & 0 \\ 0 & 0 & 0 & 0 & 0 & 3.42 & -3.35 & 0 & 0 & 0 & 0 & 0 \\ 0 & 0 & 0 & 0 & 0 & 0 & 3.35 & -3.29 & 0 & 0 & 0 & 0 \\ 0 & 0 & 0 & 0 & 0 & 0 & 0 & 3.29 & -2.86 & 0 & 0 & 0 \\ 0 & 0 & 0 & 0 & 0 & 0 & 0 & 0 & 2.86 & -2.88 & 0 & 0 \\ 0 & 0 & 0 & 0 & 0 & 0 & 0 & 0 & 0 & 2.88 & -2.83 & 0 \\ 0 & 0 & 0 & 0 & 0 & 0 & 0 & 0 & 0 & 0 & 2.83 & -2.46 \\ 0 & 0 & 0 & 0 & 0 & 0 & 0 & 0 & 0 & 0 & 0 & 2.46 \end{bmatrix} \times 10^3 \text{kN/m}. \quad (21)$$

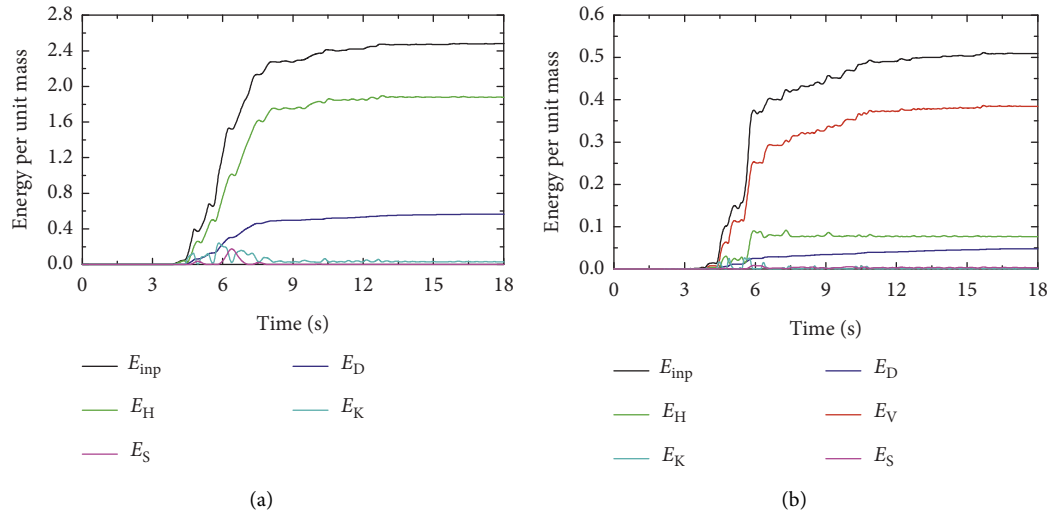

Figure 8: Time-history energy response of the SDOF structure subjected to pulse excitation: (a) uncontrolled structure and (b) structure with VDs.

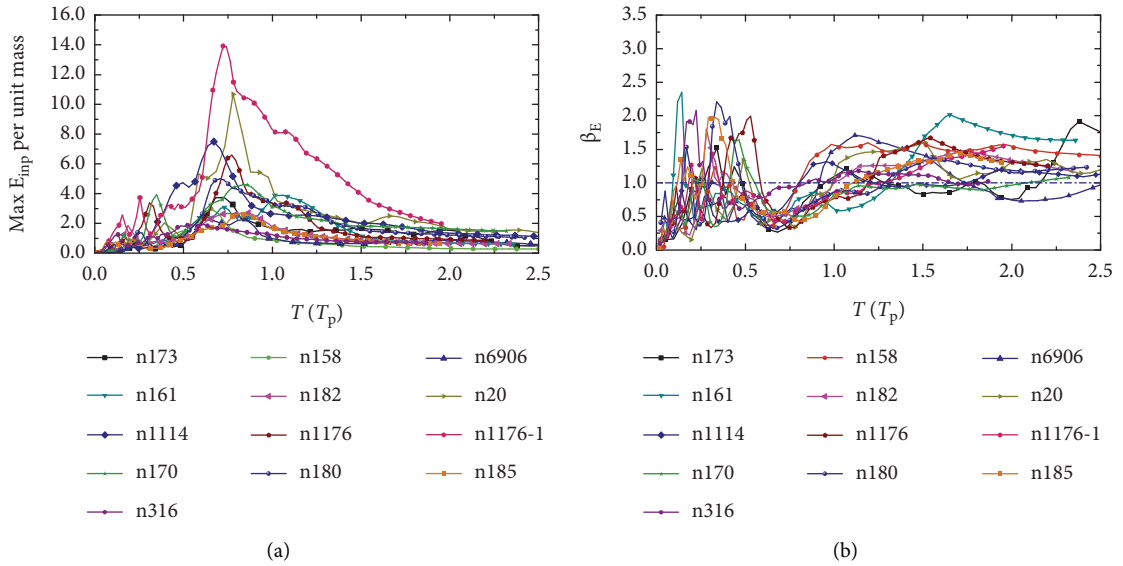

Figure 9: Max seismic input energy of structures subjected to some pulse excitations: (a) uncontrolled structure and (b) structure with VDs.

5.1. Modal Analysis of MDOF Structure. To investigate the dynamic characteristic of this frame, the first three mode shapes of the structure in X direction are presented in Figure 11 when the structure enters into different states: the elastic structure in Figure 11(a), elastoplastic structure with yield of the first storey in Figure 11(b), elastoplastic structure with yield of the first to third storeys in Figure 11(c), and elastoplastic structure with yield of the first to sixth storeys in Figure 11(d). It is observed from Figure 11(a) that the modal participating mass ratio of the first three mode shapes is more than 90%, which indicates that the response contributions of the three modes are enough to obtain the exact value of the structural response. When the first storey of the frame yields, the first mode shape is characterized by translational motion, as shown in Figure 11(b).

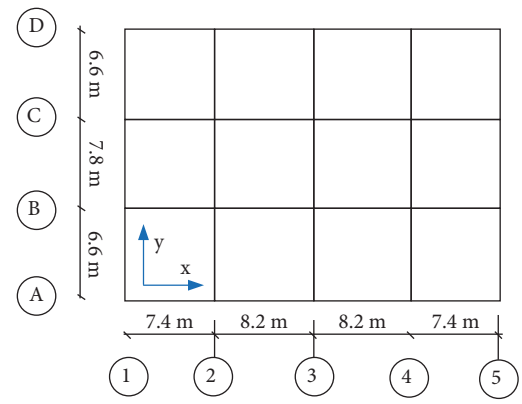

Figure 10: Plane layout of the steel structure.

Table 2: Cross sections of beams and columns.

Structural component	Storey	Location	Section (mm)
Beam	1~12 storey	1, 5 axis	HM 600×300×12×20
		2~4 axis	HM 600×300×12×32
		A ~ *D* axis	HN 600×200×11×17
Column	1~3 storey	Border column	□600×38
	4~8 storey		□600×30
	9~12 storey		□500×14
	1~4 storey	Middle column	□600×25
	5~8 storey		□500×14
	9~12 storey		□500×10

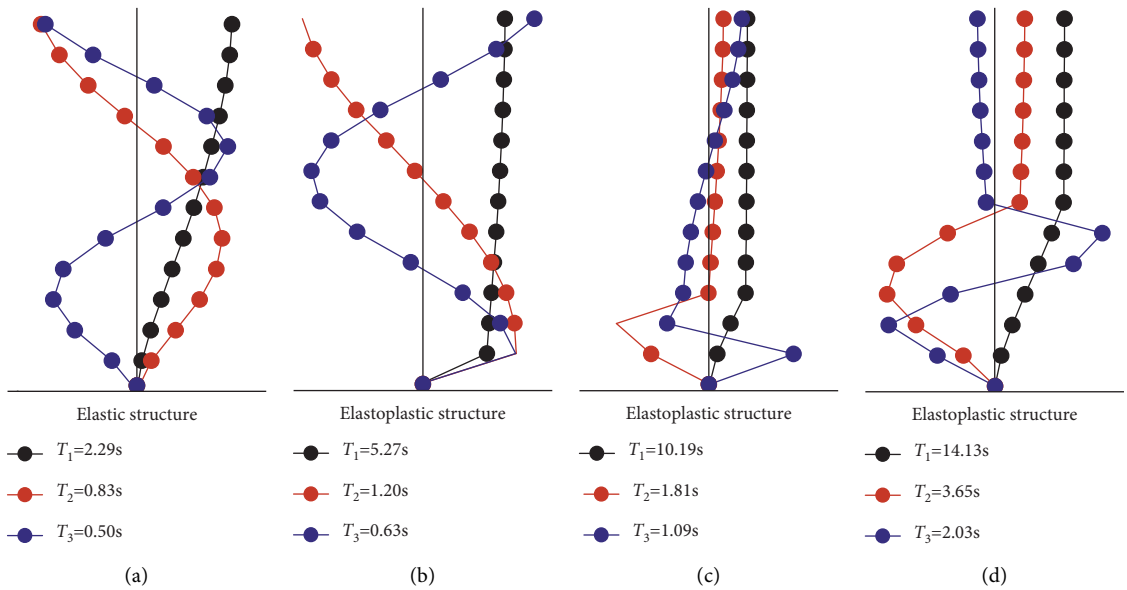

Figure 11: The first three mode shapes of the steel frame and its corresponding periods T1 ~ T3 in *X* direction: (a) elastic structure; (b) elastoplastic structure with yield of the first storey; (c) elastoplastic structure with yield of the first to third storeys; (d) elastoplastic structure with yield of the first to sixth storeys.

Furthermore, the amplitude of the mode shapes is mainly grouped in the yielded storeys when the storeys yield gradually from bottom to top of the structure, which is shown in Figures 11(c) and 11(d). In summary, it can be concluded that when the structure enters into an elastoplastic state, its dynamic characteristic is quite different from that of its corresponding elastic structure, and its displacements of the storeys that are in an elastic state are significantly reduced by shifting the response to the other storeys that are in an elastoplastic state.

5.2. Seismic Response and Its Characteristic. In this section, to show the effect of NPGM on the frame, the nonlinear time history analysis is employed to evaluate the performance of the structure under pulse-type excitations in *X* direction. The structure is excited by the ground motions shown in Table 1, and their peak ground accelerations (PGA) are scaled down to 0.4 g to commensurate with the PGA under major earthquakes of intensity 8, and the results are shown in Figure 12.

Figure 12 shows the plots of the interstorey drifts and accelerations of the structure. It is observed from Figure 12(a) that the range of interstorey drifts under NPGM in *X* direction is large and most of them exceed the Chinese code limitation, but this trend of change is basically similar. Furthermore, it can be found from the average interstorey drifts of the corresponding G1~G4 groups that the structural interstorey drifts under G1 group are small, while it gradually increases and exceeds the code limitation 1/50 under G2~G4 groups with the increase in pulse periods. It indicates that this kind of ground motions with a large pulse period can cause serious damage to the structure, and the damage is mainly concentrated in the middle and lower storeys of the structure. At the same time, it can be found that the structural average accelerations under the corresponding G1~G4 groups are similar, as shown in Figure 12(b), which implies that the PGA is not a good intensity measure to quantify the damage potential of pulse-type ground motions although it can affect the structural seismic response.

In order to investigate the vibration reduction performance of the structure with VDs under pulse-type ground

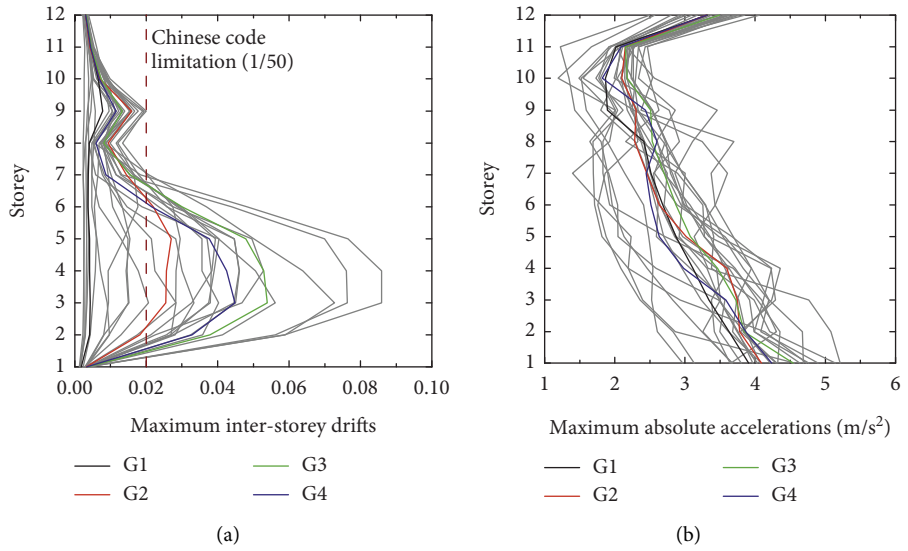

Figure 12: Maximum seismic response of the steel frame: (a) maximum interstorey drifts and (b) maximum absolute accelerations.

Table 3: Parameters of viscous dampers.

Storey	1~6	7~8	9~12
Damping coefficient of dampers c_d(kN·s/m)	9000	6000	3000
Exponent α_0	0.45	0.45	0.45

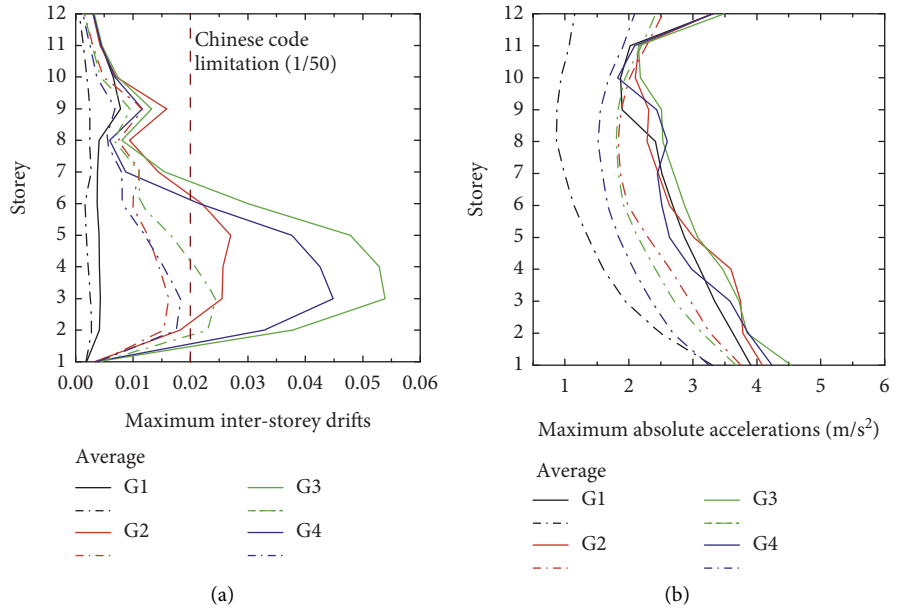

Figure 13: Comparisons of maximum seismic response of the steel frame with and without VDs: (a) maximum interstorey drifts and (b) maximum absolute accelerations. (—represent the structure without VDs; -·-represent the structure with VDs).

motions, the number of dampers and configurations are presented in Table 3 based on the above analysis, and the results of the nonlinear time history analysis are shown in Figure 13.

Figures 13(a) and 13(b) present the comparisons of maximum seismic responses of the steel frame with and without VDs. It can be found that the maximum interstorey drifts and maximum absolute accelerations are significantly

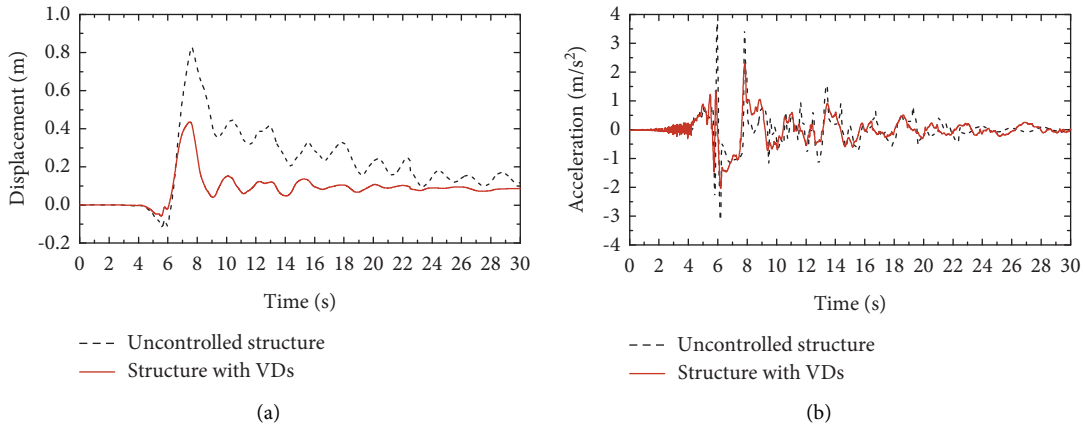

Figure 14: Time history responses at the fourth storey of the steel frame with and without VDs under the pulse-type excitation of record n180: (a) displacement time history and (b) acceleration time history.

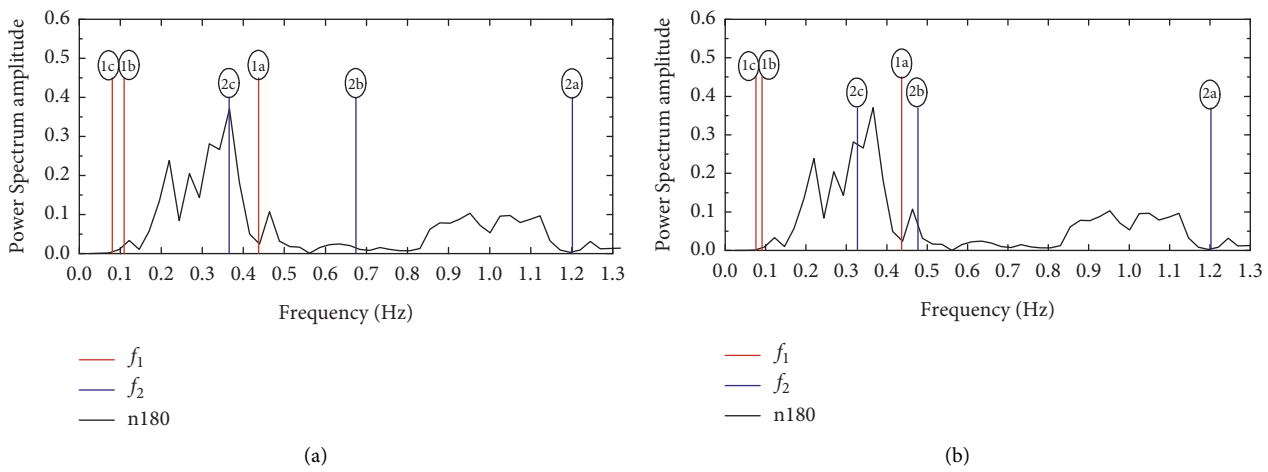

Figure 15: (a) The power spectrum of the record n180 and main natural frequencies of the uncontrolled structure (1a, 2a indicate elastic structure; 1b, 2b indicate the structural second to third storeys of yield; 1c, 2c indicate the structural second to fifth storeys yield); (b) the power spectrum of the record n180 and main natural frequencies of the structure with VDs (1a, 2a indicate elastic structure; 1b, 2b indicate the structural yield of the second to fourth storeys; 1c, 2c indicate the structural first to fifth storeys yield). *F*1 and *f*2 are the first and second natural frequencies, respectively.

reduced when the structure is equipped with VDs, and the responses are not amplified under any pulse-type excitation, which is completely different from the elastoplastic response characteristics of the SDOF structure. However, the maximum interstorey drifts of some stories still exceed the code limitation under some pulse-type excitations. This result implies that the seismic performance of the structure can be significantly improved by applying VDs, but its demand for dampers is enormous, and the structure still has the risk of local failure, even overall collapse under some pulse-type excitations. Now, record no. n180 obtained from the 1979 Imperial Valley earthquake is taken as an example to carry out a detailed analysis.

The maximum interstorey drift of the uncontrolled structure under pulse-type excitation of record n180 is 0.0859, and it occurs at the fourth storey, while it decreased from 0.086 to 0.037 when the structure is equipped with VDs. Figures 14(a) and 14(b) show the plots of the time history of displacement and acceleration at the fourth storey. It is observed that the responses of displacement and acceleration are significantly reduced when the structure is equipped with VDs, but it still appears permanent deformation. The main reason for the results is that the main energy of the record is in a relatively narrow and low-frequency band, and most stories of the structure gradually yield under a certain intensity of the record, which leads to an obvious reduction in the structural main natural frequencies. When the structural main natural frequencies approached the frequency band which the main energy of the record concentrated in, it may cause resonance and serious damage to the structure. Such as in Figure 15(a), when the structural second to fifth storeys yielded, the second natural frequency f_2(2c) of the structure is just in the frequency band where the peak energy is recorded.

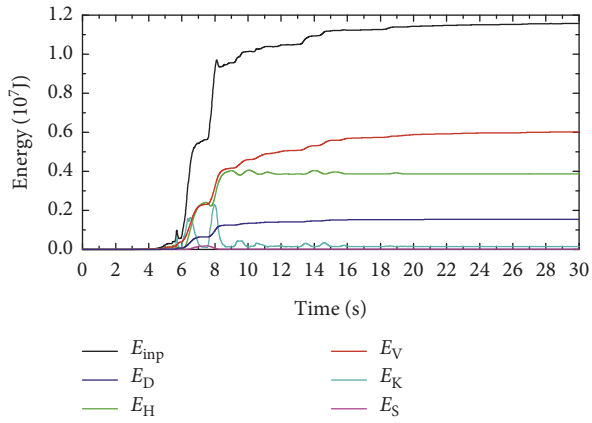

Figure 16: Time history response of energy for the steel frame with VDs under the pulse-type excitation of record n180.

However, the main natural frequencies are changed when the MDOF structure is equipped with VDs, as shown in Figure 15(b), which can help to alleviate these adverse effects.

Figure 16 shows the time history plot of the energy for the steel frame with VDs, at the same time, combined with the deformation characteristics of the structure in Figure 14(a); it can be found that the seismic input energy of n180 increases sharply in the range of 6.0–8.0 s, and it is difficult for the damper to dissipate the high instantaneous input energy generated by the record in a short time. The energy dissipation rate of the damper obviously lagged behind the increase rate of the seismic input energy of the record, which led to an increase in the plastic strain energy of the structure. This characteristic is unlike SDOF structure with VDs in Figure 8(b), and it demonstrates that the characteristics of action mechanism and seismic response of the MDOF structure are completely different from that of the SDOF structure with VDs.

6. Conclusions

In this article, the vibration reduction performance of structures with viscous dampers under near-field pulse-type ground motions has been examined via response spectrum and energy balance analysis, and the influence of various factors, such as parameters of VD, nonlinear parameter of structure, and the characteristic of ground motions, are considered. The characteristics of seismic response and energy dissipation of SDOF structure and MDOF structure are compared, which have been employed to further reveal the action mechanism of pulse-type ground motions on structures with VDs. The main conclusions of this research are the following:

(1) The parameter $k_b/(c_d\omega)$ has a significant impact on the vibration reduction performance of the structure. It is recommended that the minimum value of $k_b/(c_d\omega)$ should not be less than 6 when α_0 equals 0.3, and $k_b/(c_d\omega)$ should not be less than 3 when α_0 equals 1.0.

(2) The MDOF structure with VDs will enter into an elastoplastic state under most of pulse-type ground motions, and its main natural frequencies are constantly changing, which make its dynamic performances more complicated than that of the SDOF structure. The characteristics of vibration reduction of the SDOF structure with VDs under pulse-type ground motions may not be applicable to the MDOF structure due to its more complicated dynamic behaviours.

(3) The viscous damper can significantly reduce the seismic response of the structure under pulse-type ground motions, but the required number of VDs is enormous, and the structure with VDs may still be difficult to completely dissipate the instantaneous input energy in a short time when it is subjected to a pulse-type ground motion with a high pulse period. Usually, it can cause the structure to be damaged or even collapsed in a moment when the energy dissipation rate of the damper obviously lagged behind the increase rate of the seismic input energy of the record.

Data Availability

The data used to support the findings of this study are included within the article.

Conflicts of Interest

The author declares that there are no conflicts of interest or personal relationships that could have appeared to influence the work reported in this article.

References

[1] T. T. Soong, G. F. Dargush, *Passive Energy Dissipation Systems in Structural Engineering*, Wiley, New York, Ny, USA, 1997.

[2] T. T. Soong and B. F. Spencer, "Supplemental energy dissipation: state-of-the-art and state of-the-practice," *Engineering Structures*, vol. 24, pp. 243–259, 2002.

[3] M. C. Constantinou, T. T. Soong, and G. F. Dargush, *Passive Energy Dissipation Systems for Structural Design and Retrofit*, Multidisciplinary Center for Earthquake Engineering Research, State University of New York at Buffalo, New York, NY, USA, 1998.

[4] A. Pazooki, A. Goodarzi, A. Khajepour, A. Soltani, and C. Porlier, "A novel approach for the design and analysis of nonlinear dampers for automotive suspensions," *Journal of Vibration and Control*, vol. 24, no. 14, pp. 3132–3147, 2017.

[5] H. Houston and H. Kanamori, "Source characteristics of the 1985 Michoacan, Mexico Earthquake at periods of 1 to 30 seconds," *Geophysical Research Letters*, vol. 13, no. 6, pp. 597–600, 1986.

[6] T. H. Heaton, B. T. Aagaard, and J. F. Hall, "Effect of Fault Dip and Slip Rake Angles on Near-Source Ground Motions: Why Chi-Chi Was a Mild M 7.6 Earthquake," in *Proceedings of the AGU Fall Meeting*, San Francisco, CA, USA, December 2001.

[7] V. V. Bertero, S. A. Mahin, and R. A. Herrera, "Aseismic design implications of near-fault San Fernando earthquake

records," *Earthquake Engineering & Structural Dynamics*, vol. 6, no. 1, pp. 31–42, 1978.

[8] W. I. Liao, C. H. Loh, and S. Wan, "Earthquake responses of RC moment frames subjected to near-fault ground motions," *The Structural Design of Tall Buildings*, vol. 10, no. 3, pp. 219–229, 2001.

[9] B. Alavi and H. Krawinkler, "Behavior of moment-resisting frame structures subjected to near-fault ground motions," *Earthquake Engineering & Structural Dynamics*, vol. 33, no. 6, pp. 687–706, 2004.

[10] P. K. Malhotra, "Response of buildings to near-field pulse-like ground motions," *Earthquake Engineering & Structural Dynamics*, vol. 28, no. 11, pp. 1309–1326, 1999.

[11] R. Sehhati, A. Rodriguez-Marek, M. Elgawady, and W. F. Cofer, "Effects of near-fault ground motions and equivalent pulses on multi-storey structures," *Engineering Structures*, vol. 33, no. 3, pp. 767–779, 2011.

[12] V. Dimakopoulou, M. Fragiadakis, and C. Spyrakos, "Influence of modeling parameters on the response of degrading systems to near-field ground motions," *Engineering Structures*, vol. 53, no. 8, pp. 10–24, 2013.

[13] M. D. Symans, F. A. Charney, A. S. Whittaker et al., "Energy dissipation systems for seismic applications: current practice and recent developments," *Journal of Structural Engineering*, vol. 134, no. 1, pp. 3–21, 2008.

[14] S. Kumar and S. K. Chakraborty, "Reduction of seismic vibration in multistorey structures retrofitted with nonlinear viscous dampers using mode summation method," *Applied Mathematical Modelling*, vol. 86, pp. 294–310, 2020.

[15] E. Güler and C. Alhan, "Performance limits of base-isolated liquid storage tanks with/without supplemental dampers under near-fault earthquakes," *Structures*, vol. 33, no. 4, pp. 355–367, 2021.

[16] S. Yaghmaei-Sabegh, E. Jafari-Koucheh, and M. Ebrahimi-Aghabagher, "Estimating the seismic response of nonlinear structures equipped with nonlinear viscous damper subjected to pulse-like ground records," *Structures*, vol. 28, no. 6, pp. 1915–1923, 2020.

[17] Z. Xu, A. K. Agrawal, W. l He, and P. Tan, "Performance of passive energy dissipation systems during near-field ground motion type pulses," *Engineering Structures*, vol. 29, no. 2, pp. 224–236, 2007.

[18] J. Yi, J. Zhou, and X. Ye, "Seismic control of cable-stayed bridge using negative stiffness device and fluid viscous damper under near-field ground motions[J]," *Journal of Earthquake Engineering*, vol. 2, pp. 1–18, 2020.

[19] W. H. Lin and A. K. Chopra, "Earthquake response of elastic SDF systems with non-linear fluid viscous dampers," *Earthquake Engineering & Structural Dynamics*, vol. 31, no. 9, pp. 1623–1642, 2002.

[20] R. K. Goel, "Seismic Response Control of Irregular Structures Using Nonlinear dampers," in *Proceedings of the 13th World Conference on Earthquake Engineering*, Canada, 2004.

[21] G. Pekcan, J. B. Mander, and S. S. Chen, "Fundamental considerations for the design of non-linear viscous dampers," *Earthquake Engineering & Structural Dynamics*, vol. 28, no. 11, pp. 1405–1425, 1999.

[22] D. Losanno, J. Londono, S. Zinno, and G. Serino, "Effective damping and frequencies of viscous damper braced structures considering the supports flexibility," *Computers & Structures*, vol. 207, pp. 121–131, 2018.

[23] G. Hu, Y. Wang, W. Huang, B. Li, and B. Luo, "Seismic mitigation performance of structures with viscous dampers under near-fault pulse-type earthquakes," *Engineering Structures*, vol. 203, no. 15, Article ID 109878, 2020.

[24] L. Ming, X. Lili, Z. Changhai, and Y. Yang, "Scope division of near-fault ground motion," *Earthquake Engineering and Engineering Vibration*, vol. 29, no. 5, pp. 20–25, 2009, in Chinese.

[25] J. W. Baker, "Quantitative classification of near-fault ground motions using wavelet analysis," *Bulletin of the Seismological Society of America*, vol. 97, no. 5, pp. 1486–1501, 2007.